Quantitative mobility evaluation of organic semiconductors using quantum dynamics based on density functional theory

Hiroyuki Ishii,[1,*] Jun-ichi Inoue,[2] Nobuhiko Kobayashi,[1] and Kenji Hirose[3]

[1]*Division of Applied Physics, Faculty of Pure and Applied Sciences, University of Tsukuba, 1-1-1 Tennodai, Tsukuba, Ibaraki 305-8573, Japan*

[2]*MANA, National Institute for Materials Science, Tsukuba, Ibaraki 305-0044, Japan*

[3]*System Platform Research Laboratories, NEC Corporation, 34 Miyukigaoka, Tsukuba, Ibaraki 305-8501, Japan*

(Received 5 April 2018; revised manuscript received 30 July 2018; published 20 December 2018)

We present an order-N methodology to evaluate mobilities of charge carriers coupled with molecular vibrations using quantum dynamics based on first-principles calculations that can be applied to micron-scale soft materials. As a demonstration, we apply it to several organic semiconductors and show that the calculated intrinsic hole mobilities and their temperature dependences are quantitatively in good agreement with those obtained in experiments. We also clarified which vibrational modes dominate the transport properties. The methodology paves the way for quantitative prediction of the transport properties of various soft materials.

DOI: 10.1103/PhysRevB.98.235422

I. INTRODUCTION

The performance of materials used in electronic devices is characterized by the charge-carrier mobility and its temperature dependence. In particular, for soft materials such as organic semiconductors [1,2], conductive polymers [3,4], and biomolecular wires [5], the coupling between electrons and molecular vibrations, i.e., dynamical disorder, has been widely recognized as a key factor dominating the charge transport property. For a wide range of applications of organic electronics, such as radio-frequency identifier tags and sensors, the development of new organic semiconductors with a charge-carrier mobility in excess of 10 cm^2/Vs has been desired [6]. Although some promising organic semiconductors have been reported, which include pentacene [7], [1]benzothieno[3,2-b][1]benzothiophene (BTBT) [8], dinaphtho[2,3-b:2',3'-f]thieno[3,2-b]thiophene (DNTT) [9], and their derivatives, an outstanding issue is to systematically understand the relationship between the crystal structure and the intrinsic charge transport properties for each material. However, the intrinsic mobility is difficult to uniquely determine in experiments. This is because measured mobilities depend on the employed device architecture and its quality. Therefore, quantitatively accurate theoretical approaches to treating and predicting the intrinsic mobility of soft materials are strongly desired.

When theoretically considering the mechanisms of charge transport, two conventional models have been widely used: incoherent hopping model and coherent band-transport model. The former is applicable in the case of strong electron-vibration coupling compared with the intermolecular electronic coupling, and is described by Marcus theory. The latter describes the transport of charges weakly coupled with molecular vibrations. It is difficult to understand the transport properties using the above conventional models since several experimental studies involving Hall effect measurements [10–13], electron-spin resonance [14,15], photoelectron spectroscopy [16,17], and charge-modulation spectroscopy [18] indicate the intermediate properties between the hopping and the band limit. Toward overcoming this problem, some model studies have recently been reported. A coherent polaron model assumes that charge carriers dressed by phonon clouds create the quasiparticle band states and that coherent polarons are scattered by static disorder [19,20]. A quantum dynamical approach coupled with molecular dynamics showed that the localization of charge carriers by the large dynamical disorder of transfer integrals induced by intermolecular vibrations plays an important role at room temperature [2,21–25]. A model Hamiltonian describing both polaron formation and the dynamical disorder [26] and a flexible surface-hopping model [27], where decoherent events are introduced into the quantum dynamics, have also been proposed. These approaches treat electron-vibration coupling nonperturbatively beyond the conventional models but have been applied to one-dimensional models, which is too simple to represent the electronic and vibronic states of two-dimensional organic semiconductors. Therefore, evaluation of the intrinsic mobility with an accuracy comparable to that of experiments is still a difficult task.

In this paper, on the basis of our previous order-N simulation technique called the time-dependent wave-packet diffusion (TD-WPD) method [28], we propose a numerical method to obtain accurate mobility of charge coupled with molecular vibrations for two-dimensional organic semiconductors. The accuracy can be seen in Table I, listing mobilities of several organic semiconductors. Essentially, we calculate the hole mobility of realistic two-dimensional organic semiconductors from the velocity-velocity correlation function, instead of the mean-square displacement conventionally used [2,22,23]. Due to this approach, previously known computational difficulties, not only quantitative but also qualitative, have been overcome.

*ishii@bk.tsukuba.ac.jp

TABLE I. Hole mobilities μ_{TDWPD} ($\mathrm{cm}^2/\mathrm{Vs}$) of listed organic semiconductors at 300 K obtained by the present method. For comparison, we give the hopping mobilities μ_{hop}, band mobilities μ_{band}, and experimentally measured mobilities μ_{exp} of the organic single crystals at room temperature.

	Calculations					Experiments	
	μ_{TDWPD}	μ_{hop}	[Ref.]	μ_{band}	[Ref.]	μ_{exp}	[Ref.]
C_8-BTBT	8.2	0.77	[49]	50[a]	[50]	10	[51]
				36	[49]	0–9.1	[52]
						3.5–6	[53]
						3.5–5	[54]
Ph-BTBT-C_{10}	29.7	–	[–]	–	[–]	13–18	[55]
Pentacene	3.0	2.07	[56]	13	[50]	5.6	[59]
		13.8	[57]	4.9	[49][c]	5.0	[60]
		0.32	[49]			0.6–2.3	[61]
		5.37	[46]			2.2	[62]
						2.0	[63]
						1.9	[64]
						0.6–1.4	[65]
						0.1–0.5	[66]
						0.3	[67]
DNTT	10.4	1.8	[68]	96[b]	[50]	4–9.4	[69]
						4–8.3	[70]
						2.5–4	[71]
Naphthalene	3.0	1.32	[46]	–	[–]	1.0	[72]
C_{10}-DNBDT							
(stand)	25.0	–	[–]	–	[–]	10–16	[73]
(sleep)	1.5	–	[–]	–	[–]	–	[–]

[a]Result for C_{12}-BTBT.
[b]Result for C_{10}-DNTT.
[c]Reference [58].

II. CALCULATION METHOD

A. Diffusion constants

The mobility of carrier with charge q is obtained from the following Einstein relation:

$$\mu_x = \frac{q D_x^{(v)}}{k_B T}, \tag{1}$$

where T is the temperature. We first calculate the diffusion constant $D_x^{(v)}$ of a charge carrier along the x direction by $D_x^{(v)} \equiv \lim_{t\to+\infty} D_x^{(v)}(t)$ using Kubo's linear response theory [29,30]. The $D_x^{(v)}(t)$ is called time-dependent diffusion coefficient and was originally defined using the velocity correlation function as

$$D_x^{(v)}(t) \equiv \frac{1}{\beta}\int_0^t ds \int_0^\beta d\lambda \; Tr\{\hat{\rho}\hat{v}_x(-i\hbar\lambda)\hat{v}_x(s)\}. \tag{2}$$

Here, the density operator is defined as $\hat{\rho} \equiv \exp(-\beta\hat{H})/\mathrm{Tr}\{\exp(-\beta\hat{H})\}$ using the Hamiltonian for charge carriers $\hat{H}$ and the inverse temperature $\beta \equiv 1/(k_B T)$. The velocity operator at time s in the Heisenberg representation is given by $\hat{v}_x(s) \equiv \hat{U}^\dagger(s)\hat{v}_x\hat{U}(s)$, where $i\hbar\hat{v}_x \equiv [\hat{H}, \hat{x}]$ and $\hat{U}(s)$ is the time-evolution operator from the initial time 0 to s. Equation (2) is computed by our previously reported order-N method [28].

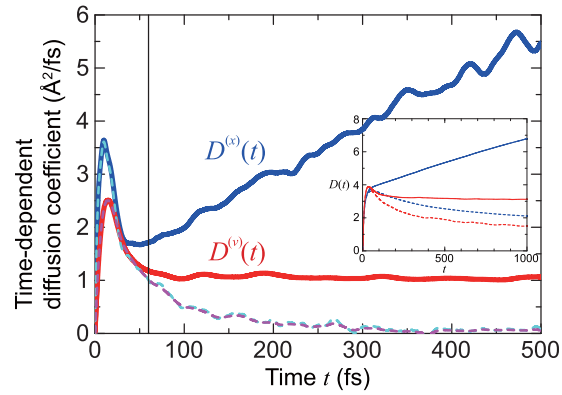

FIG. 1. Time-dependent diffusion coefficients $D^{(v)}(t)$ (red bold line) and $D^{(x)}(t)$ (blue bold line) at 300 K for a simple one-dimensional model Hamiltonian [22,33]. The vertical line represents the characteristic time of vibrations $1/\omega_0$. To compare the effects of dynamical disorder and static disorder ($\omega_0 = 0$), the diffusion coefficients in the presence of static disorder are shown by the broken lines. Inset: Time-dependent diffusion coefficients $D^{(v)}(t)$ (red) and $D^{(x)}(t)$ (blue) at 300 K for two-dimensional square lattice.

The above $D^{(v)}(t)$ is often identified with a counterpart, $D^{(x)}(t)$ defined as the mean-square displacement [2,22,23,31,32],

$$D_x^{(x)}(t) = \frac{1}{2}\frac{d}{dt}(\mathrm{Tr}[\hat{\rho}\{\hat{x}(t) - \hat{x}(0)\}^2]), \tag{3}$$

where $\hat{x}(t) \equiv \hat{U}^\dagger(t)\hat{x}\hat{U}(t)$. It is the case only when a steady-state condition is fulfilled, otherwise not. Equation (2) can be rewritten as $D_x^{(v)}(t) = \int_0^t ds \; \langle v_x(0)v_x(s)\rangle$ using the correlation between the velocities at two different real times if we regard $\{\hat{v}_x(-i\hbar\lambda)\hat{v}_x(s)\}$ to be $\{\hat{v}_x(0)\hat{v}_x(s)\}$ [29,30]. In fact, we numerically confirmed that the time-dependent diffusion coefficient calculated by $\{\hat{v}_x(0)\hat{v}_x(s)\}$ agrees with that by $\{\hat{v}_x(-i\hbar\lambda)\hat{v}_x(s)\}$ in a long-time limit. The equality $\langle v_x(0)v_x(s)\rangle = \langle v_x(t-s)v_x(t)\rangle$ is satisfied if the system is in *a steady state*. Then, after performing the time integral of $\int_0^t ds \; \langle v_x(t-s)v_x(t)\rangle$, we obtain Eq. (3), and thus $D^{(v)}(t) = D^{(x)}(t)$ at longer times under the steady-state condition.

To demonstrate the effectiveness of the present methodology, we evaluate the time evolution of the diffusion coefficients for a simple model [22,33] representing typical organic semiconductors with $\hat{H}$ as a function of γ^0 and ω_0, where the intermolecular transfer integrals γ^0 are modulated by molecular vibrations with a finite frequency of ω_0. Effects of the dynamical modulations are taken to dynamics of wave packets through the time-evolution operator $\hat{U}(t)$ in both approaches by Eqs. (2) and (3). The main (inset) panel in Fig. 1 shows the result for a one- (two-) dimensional system. The red and blue bold lines in each show $D^{(v)}(t)$ and $D^{(x)}(t)$, respectively. Obviously, these two behave differently: $D^{(x)}(t)$ diverges as $t \to \infty$. Note that two quantities in the absence of dynamical disorder ($\omega_0 = 0$), as shown by broken lines, are decreasing with time passing, and are expected to become a same value in long-time limit [34]. The negative slope implies that carriers are scattered backward by the static disorder, then the diffusion coefficients steadily decrease, showing the typical behavior of Anderson localization.

In the presence of dynamical disorder ($\omega_0 > 0$), the results follow Anderson localization behavior at much shorter timescale $t \sim 1/\omega_0$ since the disorder can be regarded as static. After that, the dynamical disorder should destroy the localized states. Ciuchi *et al*. introduced the transient localization scenario to describe it and characterized the charge transport of organic semiconductors [22]. In their study, the diffusion coefficient was evaluated using $D^{(x)}(t)$, therefore they suffered from the divergence at the long-time limit, as shown by the blue line in Fig. 1. They ascribed this divergence to the progressive heating of the electronic system, owing to the excess energy being constantly injected by the molecular vibrations. To evade the divergence and define a diffusion constant at large t, they introduced an artificial damping factor in Eq. (3) and obtained a constant value. Note that an exact treatment of electron-vibration coupling [33] may eliminate the heating problem but requires an impractically large computational cost.

On the other hand, $D^{(v)}(t)$, the original definition of the diffusion coefficient based on the Kubo formalism converges to a constant value as shown in Fig. 1, without any artificial treatment. The point of qualitatively different behavior between $D^{(x)}(t)$ and $D^{(v)}(t)$ lies in whether the steady-state condition, $\langle v_x(0)v_x(s)\rangle = \langle v_x(t-s)v_x(t)\rangle$, holds or not. This condition breaks down when the electronic system is constantly heated by molecular vibrations, and $D^{(x)}(t)$ ceases from a diffusion constant [35,36]. As such, the choice of employing $D^{(v)}(t)$ is natural and practically useful to avoid the heating problem.

B. Coupling between electrons and molecular vibrations

We apply the present methodology using Eqs. (1) and (2) to organic semiconductors. The electron propagation in a molecular crystal is determined by its interaction with the inter- and intramolecular vibrations. To construct a Hamiltonian $\hat{H}$ that properly accounts for these interactions, we must separate slow from fast interactions with respect to the characteristic time of electron dynamics [26]. The time for Bloch wave formation has been estimated to be longer than $h/\gamma^0 \simeq 40$ fs since the bare transfer integrals γ^0 of typical organic semiconductors are smaller than 0.1 eV. The intramolecular vibrations strongly coupled with the π electron states of a molecule have frequencies ω^{intra} from 1000 to 1600 cm^{-1} (0.12 to 0.20 eV) [37], which correspond to intramolecular carbon stretching modes. Since these fast interactions arise prior to the formation of the Bloch wave, they have the effect of dressing the charge with an intramolecular distortion cloud, consequently leading to renormalization of the bare transfer integrals, called the band-narrowing effect, by polaron formation [19,26]. On the other hand, the intermolecular vibrations, such as the translational mode of rigid molecules, have a characteristic time much longer than h/γ^0 because these frequencies ω^{inter} range from 0 to 100 cm^{-1} (0 to 0.012 eV). The slow and large intermolecular vibrations scatter the Bloch waves and induce transient localization as shown in Fig. 1 [22].

The time-dependent Hamiltonian of a hole coupled with inter- and intramolecular vibrations is written as

$$\hat{H}(t) = \sum_{N,M} \gamma_{NM}(t)(\hat{a}_N^\dagger \hat{a}_M + \hat{a}_M^\dagger \hat{a}_N) + \sum_N \varepsilon_N \hat{a}_N^\dagger \hat{a}_N, \quad (4)$$

where ε_N represents the energy level of the Nth molecular orbital. The operators $\hat{a}_N$ and $\hat{a}_N^\dagger$ are the annihilation and creation operators of a hole at Nth orbital. The effective transfer integrals between the Nth and Mth orbitals are given by

$$\gamma_{NM}(t) = \alpha^{\text{intra}}\left\{\gamma^0_{NM} + \alpha^{\text{inter}}_{NM}(t)\right\}, \quad (5)$$

$$\alpha^{\text{inter}}_{NM}(t) = \sum_{l,\mathbf{q}} \Delta\gamma^{\text{inter}}_{NMl\mathbf{q}} \sin\left(\omega^{\text{inter}}_{l\mathbf{q}} t + \mathbf{q}\cdot\mathbf{R}_\xi + \phi_{l\mathbf{q}}\right), \quad (6)$$

where γ^0 represents the bare transfer integral. Here we employ the all-atom normal-mode analysis beyond the rigid-molecule approximation. The effects of intermolecular vibrations on the transfer integrals are introduced in $\alpha^{\text{inter}}_{NM}(t)$, which is given by the harmonic oscillation form containing the frequency $\omega^{\text{inter}}_{l\mathbf{q}}$ of lth mode with wave number $\mathbf{q}$, and initial random phase $\phi_{l\mathbf{q}}$ in Eq. (6). The amplitude of dynamical fluctuation in transfer integrals is given by

$$\Delta\gamma^{\text{inter}}_{NMl\mathbf{q}} = g(\omega_{l\mathbf{q}}) \frac{\partial\gamma^0_{NM}}{\partial \mathbf{u}^{l\mathbf{q}}} \Delta\mathbf{r}^{l\mathbf{q}}, \quad (7)$$

where the component of $\mathbf{u}^{l\mathbf{q}}$ with respect to the nth atom is defined by $\mathbf{e}_n^{l\mathbf{q}}/\sqrt{m_n}$ using the eigenvectors $\mathbf{e}^{l\mathbf{q}}$ of the dynamical matrix and the mass m_n of the nth atom. The quantity $(\partial\gamma^0_{NM}/\partial\mathbf{u}^{l\mathbf{q}})$ corresponds to the magnitude of electron-vibration coupling. The amplitude of the displacement is given by $\Delta\mathbf{r}^{l\mathbf{q}} = \sqrt{\hbar n_{l\mathbf{q}}/2\omega_{l\mathbf{q}}}\mathbf{u}^{l\mathbf{q}}$, where $n_{l\mathbf{q}}$ is the phonon number excited at temperature T [38,39]. To take only molecular vibrations slower than the Bloch wave formation into account, we introduce a filtering function $g(\omega)$ [40]. The fast intramolecular vibrations renormalize the bare transfer integral by small-polaron formation. The renormalization factor is obtained as $\alpha^{\text{intra}} = \exp\{-(\lambda/2\hbar\omega^{\text{intra}})\coth(\beta\hbar\omega^{\text{intra}}/2)\}$, where λ and ω^{intra} represent the reorganization energy and the frequency of the normal mode with the most significant contribution, respectively [41].

C. Procedure of mobility evaluation

First, we evaluate the bare transfer integrals γ^0 in Eq. (5) from the experimentally observed crystal structure. The bare transfer integrals γ^0 can be computed using Wannier [42] or dimer [37,43,44] methods based on density functional theory (DFT). Although the Wannier method requiring high computational cost gives the exact transfer integrals in comparison with the low-cost dimer method, we have confirmed that the difference in transfer integrals is less than 10 meV [32]. Therefore, to reduce the computational cost, we employ a dimer method in this paper. We take the highest occupied molecular orbitals (HOMOs) and the second HOMOs (SHOMOs) as the basis set of $\hat{H}$ because we found that the dispersion at the HOMO band top of some materials is affected by the transfer integrals between HOMO and SHOMO. We set the orbital energy of isolated single molecule as the on-site energy ε.

The normal vibrational modes of crystal, $\omega_{l\mathbf{q}}$ and $\mathbf{u}^{l\mathbf{q}}$, are obtained from the dynamical matrix constructed by the force field MMFF94s using CONFLEX [45]. The magnitude of dynamic disorder in transfer integrals induced by the

molecular vibrations is given by $\Delta\gamma^{\text{inter}}$ in Eq. (7), which is characterized by the electron-molecular vibration coupling $\partial\gamma^0/\partial\mathbf{u}^{l\mathbf{q}}$ and the amplitude of molecular vibration $\Delta\mathbf{r}^{l\mathbf{q}}$ at temperature T given above. When increasing temperature, the amplitude $\Delta\mathbf{r}^{l\mathbf{q}}$ becomes larger, resulting in enhancement of dynamic disorder in transfer integrals. Here, the quantity of $\partial\gamma^0/\partial\mathbf{u}^{l\mathbf{q}}$ for each normal vibrational mode can be computed by numerical differentiation. The λ in α^{intra} is calculated by the adiabatic potential energy surface method [46] using the B3LYP/6-31G(d) level derived by GAMESS [47]. We employ 0.15 eV as the typical value of $\hbar\omega^{\text{intra}}$ in this paper [37]. As a result, we obtain the time-dependent Hamiltonian $\hat{H}(t)$ of Eq. (4) for charge carrier coupled with molecular vibrations.

Then we evaluate the diffusion constant $D_x^{(v)}$ defined by Eq. (2) using our order-N simulation technique, called the TD-WPD method. Finally, the mobility at temperature T is evaluated using Eq. (1). We employ a monolayer consisting of 200×200 unit cells, which corresponds to single crystal with the area of $120 \times 160\ \text{nm}^2$ containing 1.6×10^5 molecular orbitals in case of C_8-BTBT. The carrier dynamics is computed up to 2 ps with a time step of 0.5 fs.

III. APPLICATION TO ORGANIC SEMICONDUCTORS

First, we evaluate the intrinsic hole mobilities along the column direction at 300 K using the present TD-WPD method for single crystals of C_8-BTBT [8], Ph-BTBT-C_{10} [48], pentacene, DNTT [9], and naphthalene, as listed in Table I. Note that the mobilities reported in the experiments had distributions to some extent even for single-crystal devices. This is because the measured mobilities depend on the employed device architecture and measurement conditions. The calculated mobilities are in good agreement with those obtained in experiments and consistent with recently reported theoretical works [25]. Remarkably, the distinguished character of hole mobilities of C_8-BTBT from Ph-BTBT-C_{10} is successfully reproduced in our calculations, as seen in Table I. It is because the phenyl groups of Ph-BTBT-C_{10} enhance intermolecular transfer integrals [74], resulting in higher mobility.

For comparison, the mobilities calculated from two limiting conventional models are listed as μ_{hop} and μ_{band} in Table I. The μ_{hop} is derived from the incoherent hopping model based on Marcus theory, [46,75] which assumes that a carrier creates a small-polaron state on a single molecule and hops to neighboring molecules without phase coherence. Marcus theory is applicable for $\lambda/4 \gg \gamma^0$, and γ^0 is comparable to λ for the organic semiconductors studied here, which implies that charge carriers are delocalized over a few molecules. Therefore, we see that the μ_{hop} is less than μ_{exp}. On the other hand, μ_{band} is derived from the band-transport model [50], which assumes that coherent Bloch waves are scattered by intermolecular vibrations. However, Anderson-localization effect is not included, thus μ_{band} is much larger than μ_{exp}.

Then, we take the recently reported molecule, decyl-substituted dinaphtho[2,3-d:2',3'-d']benzo[1,2-b:4,5-b']dithiophene (C_{10}-DNBDT) [73], which has two different crystal phases called the sleep and stand phases. We note that the mobility of the stand phase has been experimentally observed but not that of the sleep phase. To account for this, we calculate the hole mobility of the sleep phase using the experimentally obtained single-crystal structure and find that the sleep phase has a much lower mobility of 1.5 cm^2/Vs than that of 25.0 cm^2/Vs for the stand phase as shown in Table I. A sizable difference between the two phases would draw attention. An experimental result for the sleep phase should be awaited.

To investigate origins of the difference in magnitude of mobility among these materials, we show the HOMO band structures for C_{10}-DNBDT (stand), C_8-BTBT, pentacene, and C_{10}-DNBDT (sleep) in Figs. 2(a)–2(d), respectively. Here the band structures are calculated in case of no electron-molecular-vibration couplings ($\alpha^{\text{inter}} = 0$ and $\alpha^{\text{intra}} = 1$). The mobilities are computed along the column direction shown by the blue arrow in the inset of Fig. 2(e), which corresponds to the Γ–X and S–Y direction in reciprocal lattice space. The results show that electronic states of C_{10}-DNBDT (sleep) can be regarded as a one-dimensional system along the column direction, while C_{10}-DNBDT (stand) is a nearly isotropic two-dimensional electronic system. In general, localization effects induced by disorder are enhanced in a one-dimensional system rather than a two-dimensional system, which is consistent with time-dependent behavior of $D^{(v)}(t)$ as discussed below. Therefore, the mobility of C_{10}-DNBDT (sleep) becomes much lower than that of C_{10}-DNBDT (stand). An origin of large difference in magnitude of mobility between C_{10}-DNBDT (stand) and C_{10}-DNBDT (sleep) can be explained by the difference in dimensionality.

C_{10}-DNBDT (stand) and C_8-BTBT have similar isotropic two-dimensional systems with respect to the electrons and the molecular vibrations, resulting in high mobilities with bandlike transport property. It is hard to show an origin of the relatively small difference in magnitude of mobilities between both materials, because the transfer integrals γ^0, the molecular vibrations $h\omega$, and the dynamic disorder $\Delta\gamma^{\text{inter}}$ are of similar energetic order of a few 10 to 100 meV. Such relatively small difference in mobility ascribes to a delicate balance among these quantities.

Next, we move to discussion of temperature dependence of the hole mobilities. In Fig. 2(e), we present both the experimental and computational results, which show power-law behavior for C_{10}-DNBDT (stand) and C_8-BTBT while thermally activated behavior for C_{10}-DNBDT (sleep) [76]. The power-law exponents of C_{10}-DNBDT (stand) and C_8-BTBT are -0.88 and -1.44, in very good agreement with the experimental values of -0.85 and -1.1, shown in open symbols, respectively [52,77]. In contrast to those above, single-crystal pentacene is known to exhibit an intermediate character between hopping and band transport, resulting in temperature-independent mobility [66]. The present simulations also successfully reproduce this behavior, as shown in Fig. 2(f) in the temperature range from 200 to 300 K.

To clarify the origin of the different temperature dependences of the mobility for these materials, we investigate the time-dependent behavior of $D^{(v)}(t)$. Figure 2(g) shows the calculated results for pentacene, C_8-BTBT, and the stand and sleep phases of C_{10}-DNBDT. The transient localization behavior for C_{10}-DNBDT (sleep) is clearly observed, resulting in the thermally activated behavior of low mobility. On the other hand, we cannot observe the negative slope of $D^{(v)}(t)$

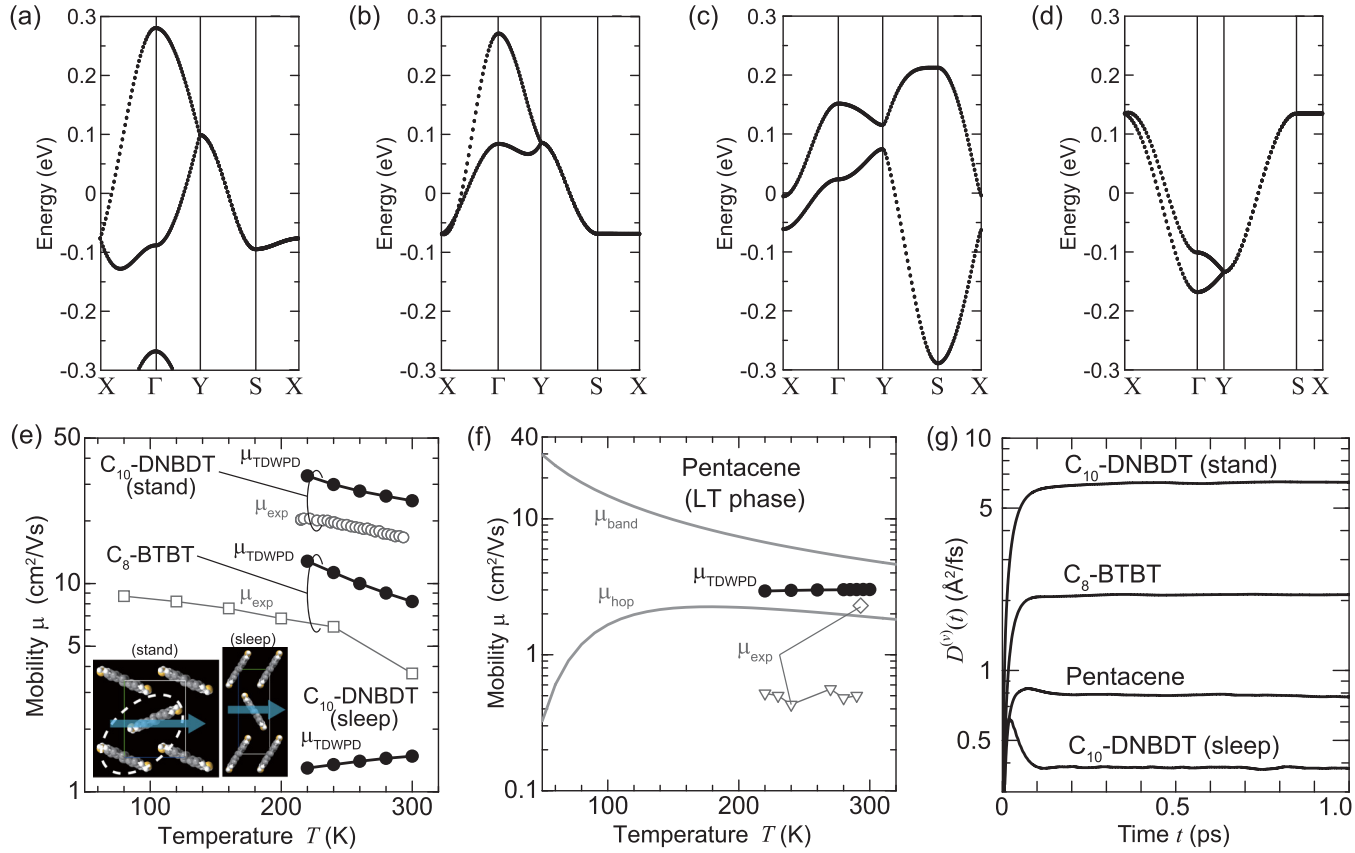

FIG. 2. (a)–(d) Calculated HOMO band structure with symmetry points of $\Gamma(0,0,0)$, $X(1/2,0,0)$, $Y(0,1/2,0)$, $S(1/2,1/2,0)$ for C_{10}-DNBDT (stand), C_8-BTBT, pentacene, and C_{10}-DNBDT (sleep), respectively. The origin of energy axis is set to the on-site energy (HOMO energy level). (e) Thermally activated μ_{TDWPD} of C_{10}-DNBDT (sleep) and power-law temperature dependence of μ_{TDWPD} of C_{10}-DNBDT (stand) and C_8-BTBT, shown by solid circles. The different crystal structures of the C_{10}-DNBDT polymorphs are shown in the insets. The alkyl side chains are omitted for visibility. The mobilities are calculated along the column direction shown by the arrow. The activation energy of the mobility for C_{10}-DNBDT (sleep) is estimated to be 9.5 meV. The experimental data points for C_{10}-DNBDT (stand) and C_8-BTBT are shown by circles [77] and squares [52], respectively. (f) Temperature-independent μ_{TDPWD} of pentacene shown by solid circles. The μ_{band} [49,58] and μ_{hop} [49] are represented by gray curves. The experimental data are plotted by diamonds [61] and triangles [66]. (g) Calculated time-dependent diffusion coefficients $D^{(v)}(t)$ at 300 K for pentacene, C_8-BTBT, and the stand and sleep phases of C_{10}-DNBDT.

for C_{10}-DNBDT (stand) and C_8-BTBT. Their time-dependent behaviors of $D^{(v)}(t)$ resemble those of ideal band transport, but we confirm that the HOMO band-edge states are spatially localized by the large dynamical disorder, owing to the intermolecular vibrations. Therefore, the calculated μ_{TDWPD} of C_8-BTBT is lower than the μ_{band}.

As discussed above, evaluations of the dynamical disorder is important to understand the intrinsic transport properties of organic semiconductors. Here, we employ C_{10}-DNBDT (stand) as an example of a promising material with high mobility, and investigate which intermolecular vibrational modes induce the large dynamic disorder. The magnitude of the modulation by lth mode with the momentum $\mathbf{q}$ is evaluated using $\Delta\gamma^{\mathrm{inter}}_{NMl\mathbf{q}}$ given by Eq. (7). Figure 3 shows $\Delta\gamma^{\mathrm{inter}}_{NMl\mathbf{q}=0}$ for the C_{10}-DNBDT (stand) dimer surrounded by the broken ellipse in the inset of Fig. 2(e). Two translational vibrations of the core part of the molecule, namely the out-of-plane mode (2.0 meV) and in-plane mode (0.4 meV), significantly modulate the transfer integrals, $\Delta\gamma^{\mathrm{inter}}_{\omega=2.0\mathrm{meV}} \approx 14$ meV, and $\Delta\gamma^{\mathrm{inter}}_{\omega=0.4\mathrm{meV}} \approx 10.5$ meV, respectively. These dynamical disorders $\Delta\gamma$ reach the same energetic order of the bare transfer

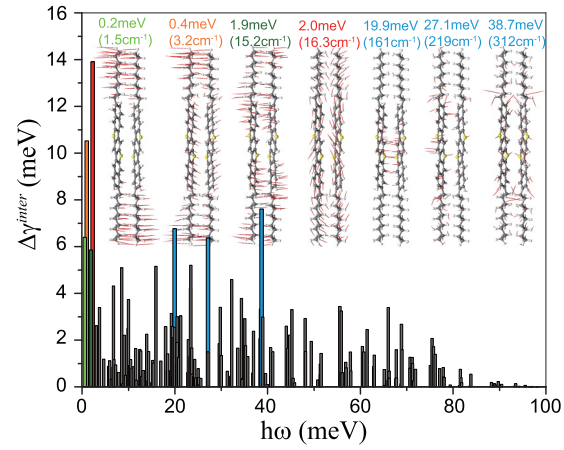

FIG. 3. Amplitudes of vibrating transfer integrals of C_{10}-DNBDT (stand) induced by the molecular vibrations with the frequencty $h\omega^{\mathrm{inter}}_{l\mathbf{q}=0}$ at 300 K. Red arrows in the schematic molecular structures represent the normal-mode coordinates with its frequencies $h\omega^{\mathrm{inter}}_{l\mathbf{q}=0}$.

integral γ^0 of 46 meV, which is enough to induce transient localization even in high-mobility materials with bandlike transport property. Therefore, it is considered that pure band-transport theory, where the dynamical disorder is treated as perturbatively, overestimates the intrinsic hole mobility. Furthermore, we found that the out-of-plane mode and in-plane mode are commonly significant for the other organic semiconductors studied here. We confirm that the result for pentacene is consistent with previous theoretical work [37]. Note that the rotational modes (0.2 meV), bending modes (1.9 meV), and the other modes also have a nonnegligible impact on the transfer integrals. This implies that when quantitatively evaluating the mobility, the all-atom normal mode analysis, instead of the rigid-body molecular dynamics well used in previous studies [2,21–23,31,32], should be required.

IV. SUMMARY

In summary, we presented an order-N methodology for the quantitative evaluation of mobility using a wave-packet dynamical approach based on DFT that can be applied to soft materials. As a demonstration, we investigated the intrinsic hole mobilities of several organic semiconductors. We confirmed that the calculated mobilities and their temperature dependences are quantitatively in good agreement with those obtained in experiments. The essence of the requirements to quantitatively evaluate mobility is employing the proper computation method of diffusion coefficient defined using the velocity correlation function. Moreover, quantitatively accurate evaluations of both two-dimensional transfer-integral networks based on DFT and effects of dynamic disorder induced by all phonon modes on the electronic states are also required. Since our methodology enables quantitative prediction of the transport properties of various soft materials using first-principles calculations, we believe that it becomes a powerful tool when developing new materials.

ACKNOWLEDGMENTS

We thank Dr. S. Obata, Prof. H. Goto, Prof. T. Okamoto, and Prof. J. Takeya for valuable data, comments, and suggestions. We acknowledge JSPS KAKENHI Grants No. JP15H05418, No. JP18H01856, No. JP17H02780, No. JP17H06123, No. JP17H03104, and No. JP26105011. Numerical calculations were performed at the Center for Computational Sciences, University of Tsukuba and the Supercomputer Center, the Institute for Solid State Physics, the University of Tokyo.

[1] P. Gosar and S.-I. Choi, Phys. Rev. **150**, 529 (1966).
[2] A. Troisi and G. Orlandi, Phys. Rev. Lett. **96**, 086601 (2006).
[3] H. Shirakawa, E. J. Louis, A. G. MacDiarmid, C. K. Chiang, and A. J. Heeger, J. Chem. Soc. Chem. Commun. 578 (1977).
[4] W. P. Su, J. R. Schrieffer, and A. J. Heeger, Phys. Rev. Lett. **42**, 1698 (1979).
[5] R. Gutiérrez, R. A. Caetano, B. P. Woiczikowski, T. Kubar, M. Elstner, and G. Cuniberti, Phys. Rev. Lett. **102**, 208102 (2009).
[6] C. D. Dimitrakopoulos and P. R. L. Malenfant, Adv. Mater. **14**, 99 (2002).
[7] D. J. Gundlach, Y. Y. Lin, T. N. Jackson, S. F. Nelson, and D. G. Schlom, IEEE Electron Device Lett. **18**, 87 (1997).
[8] H. Ebata, T. Izawa, E. Miyazaki, K. Takimiya, M. Ikeda, H. Kuwabara, and T. Yui, J. Am. Chem. Soc. **129**, 15732 (2007).
[9] T. Yamamoto and K. Takimiya, J. Am. Chem. Soc. **129**, 2224 (2007).
[10] J. Takeya, K. Tsukagoshi, Y. Aoyagi, T. Takenobu, and Y. Iwasa, Jpn. J. Appl. Phys. **44**, L1393 (2005).
[11] V. Podzorov, E. Menard, J. A. Rogers, and M. E. Gershenson, Phys. Rev. Lett. **95**, 226601 (2005).
[12] J.-F. Chang, T. Sakanoue, Y. Olivier, T. Uemura, M.-B. Dufourg-Madec, S. G. Yeates, J. Cornil, J. Takeya, A. Troisi, and H. Sirringhaus, Phys. Rev. Lett. **107**, 066601 (2011).
[13] H. T. Yi, Y. N. Gartstein, and V. Podzorov, Sci. Rep. **6**, 23650 (2016).
[14] K. Marumoto, S.-I. Kuroda, T. Takenobu, and Y. Iwasa, Phys. Rev. Lett. **97**, 256603 (2006).
[15] H. Matsui, T. Hasegawa, Y. Tokura, M. Hiraoka, and T. Yamada, Phys. Rev. Lett. **100**, 126601 (2008).
[16] S.-I. Machida, Y. Nakayama, S. Duhm, Q. Xin, A. Funakoshi, N. Ogawa, S. Kera, N. Ueno, and H. Ishii, Phys. Rev. Lett. **104**, 156401 (2010).
[17] F. Bussolotti, Y. Yang, T. Yamaguchi, K. Yonezawa, K. Sato, M. Matsunami, K. Tanaka, Y. Nakayama, H. Ishii, N. Ueno, and S. Kera, Nat. Commun. **8**, 173 (2017).
[18] K. Miyata, S. Tanaka, Y. Ishino, K. Watanabe, T. Uemura, J. Takeya, T. Sugimoto, and Y. Matsumoto, Phys. Rev. B **91**, 195306 (2015).
[19] K. Hannewald and P. A. Bobbert, Phys. Rev. B **69**, 075212 (2004).
[20] F. Ortmann, F. Bechstedt, and K. Hannewald, Phys. Rev. B **79**, 235206 (2009).
[21] S. Fratini and S. Ciuchi, Phys. Rev. Lett. **103**, 266601 (2009).
[22] S. Ciuchi, S. Fratini, and D. Mayou, Phys. Rev. B **83**, 081202(R) (2011).
[23] H. Ishii, K. Honma, N. Kobayashi, and K. Hirose, Phys. Rev. B **85**, 245206 (2012).
[24] S. Fratini, D. Mayou, and S. Ciuchi, Adv. Func. Mater. **26**, 2292 (2016).
[25] S. Fratini, S. Ciuchi, D. Mayou, G. Trambly de Laissardière, and A. Troisi, Nat. Mater. **16**, 998 (2017).
[26] J.-D. Picon, M. N. Bussac, and L. Zuppiroli, Phys. Rev. B **75**, 235106 (2007).
[27] L. Wang and D. Beljonne, J. Phys. Chem. Lett. **4**, 1888 (2013).
[28] H. Ishii, H. Tamura, M. Tsukada, N. Kobayashi, and K. Hirose, Phys. Rev. B **90**, 155458 (2014).
[29] R. Kubo, J. Phys. Soc. Jpn. **12**, 570 (1957).
[30] S. Fujita, *Statistical and Thermal Physics, Part II: Quantum Statistical Mechanics and Simple Applications* (Krieger, Malabar, FL, 1986).
[31] H. Ishii, N. Kobayashi, and K. Hirose, Phys. Rev. B **88**, 205208 (2013).
[32] H. Ishii, N. Kobayashi, and K. Hirose, Phys. Rev. B **95**, 035433 (2017).

[33] The model Hamiltonian for an electron $\hat{H}$ is a function of γ^0 and ω_0, where $\gamma^0 = 0.11$ eV, $1/\omega_0 = 60$ fs, the mass of a site M is 533 u, and the spring constant K between neighboring molecules is 0.149 u/fs^2. The electron-vibration coupling α, defined by the ratio of the change in the transfer integral to the displacement, is 0.922 eV/Å with the lattice constant $a = 5$ Å. As defined in Ref. [22], the model Hamiltonian at time t is given by $\hat{H}(t) = \sum_i \{-\gamma^0 + \alpha(u_i(t) - u_{i+1}(t))\}(\hat{c}_i^\dagger \hat{c}_{i+1} + \hat{c}_{i+1}^\dagger \hat{c}_i)$, where $u_i(t)$ represents the displacement of ith molecules at time t. $u_i(t)$ can be obtained from the canonical equation of motion, $M\ddot{u}_i(t) = K(u_{i+1}(t) - 2u_i(t) + u_{i-1}(t))$. This model does not fully take the exchange of energy between molecular vibrations and charge carriers into account, so that it is less accurate than full quantum dynamical approaches [27,24]. However, since the system size studied here is larger, this is not necessarily a serious problem. The γ_0 and ω_0 dependences on diffusion constants (mobilities) are discussed in Ref. [22].

[34] In fact, we can see that $D^{(v)}(t)$ and $D^{(x)}(t)$ for one-dimensional system in the absence of dynamical disorder rapidly decrease and agree at over 40 fs. On the other hand, the slower decrease of $D^{(v)}(t)$ and $D^{(x)}(t)$ for two-dimensional systems than those for one-dimensional systems agrees to the fact that the Anderson-localization effect becomes weaker as the dimension becomes larger. It is expected that $D^{(v)}(t)$ and $D^{(x)}(t)$ of two-dimensional system also agree in long-time limit, but the D cannot access the long-time limit in the wave-packet dynamical approach due to huge computational cost.

[35] We discussed the transport properties of carbon nanotubes using $D^{(x)}(t)$ in our previous study [36]. However the discrepancy between $D^{(v)}$ and $D^{(x)}$ is negligible because of the "weak" electron-vibration coupling of carbon nanotubes.

[36] H. Ishii, N. Kobayashi, and K. Hirose, Phys. Rev. B **82**, 085435 (2010).

[37] A. Girlando, L. Grisanti, M. Masino, A. Brillante, R. G. Della Valle, and E. Venuti, J. Chem. Phys. **135**, 084701 (2011).

[38] When calculating the amplitudes $\Delta \mathbf{r}^{l\mathbf{q}}$ under a harmonic approximation, the calculated values are much larger than the experimentally observed amplitudes. Therefore, we introduce the modified phonon number $n_{l\mathbf{q}} = (e^{\beta h\omega_{l\mathbf{q}}} - 1)^{-1}$ for $n_{l\mathbf{q}} \leqslant n_{\mathrm{cutoff}}$ and $n_{l\mathbf{q}} = n_{\mathrm{cutoff}}$ for $n_{l\mathbf{q}} \leqslant n_{\mathrm{cutoff}}$. Here, n_{cutoff} is set to 3 for all materials studied in this paper. The calculated amplitudes of out-of-plane modes range from 0.1 to 0.3 Å, in good agreement with the experiment [39]. An accurate treatment of the anharmonicity for the low-frequency intermolecular vibrations is desirable as future work.

[39] S. Illig, A. S. Eggeman, A. Troisi, L. Jiang, C. Warwick, M. Nikolka, G. Schweicher, S. G. Yeates, Y. H. Geerts, J. E. Anthony, and H. Sirringhaus, Nat. Commun. **7**, 10736 (2016).

[40] $g(\omega)$ becomes zero for $h\omega \geqslant 0.1$ eV and unity for $h\omega \leqslant 0.05$ eV since the maximum value of the transfer integrals γ^0 is about 0.1 eV. In the intermediate region, $g(\omega)$ decreases linearly from unity to zero with increasing ω.

[41] H. Houili, J. D. Picon, L. Zuppiroli, and M. N. Bussac, J. Appl. Phys. **100**, 023702 (2006).

[42] C. Motta and S. Sanvito, J. Chem. Theory Comput. **10**, 4624 (2014).

[43] E. F. Valeev, V. Coropceanu, D. A. da Silva Filho, S. Salman, and J.-L. Brédas, J. Am. Chem. Soc. **128**, 9882 (2006).

[44] A. Troisi and G. Orlandi, J. Phys. Chem. A **110**, 4065 (2006).

[45] H. Goto, S. Obata, N. Nakayama, and K. Ohta, CONFLEX8, Conflex, Tokyo, Japan (2017).

[46] W.-Q. Deng and W. A. Goddard III, J. Phys. Chem. B **108**, 8614 (2004).

[47] M. W. Schmidt, K. K. Baldridge, J. A. Boatz, S. T. Elbert, M. S. Gordon, J. H. Jensen, S. Koseki, N. Matsunaga, K. A. Nguyen, S. J. Su, T. L. Windus, M. Dupuis, and J. A. Montgomery Jr., J. Comput. Chem. **14**, 1347 (1993).

[48] H. Iino, T. Usui, and J.-I. Hanna, Nat. Commun. **6**, 6828 (2015).

[49] H. Kobayashi, N. Kobayashi, S. Hosoi, N. Koshitani, D. Murakami, R. Shirasawa, Y. Kudo, D. Hobara, Y. Tokita, and M. Itabashi, J. Chem. Phys. **139**, 014707 (2013).

[50] J. E. Northrup, Appl. Phys. Lett. **99**, 062111 (2011).

[51] T. Uemura, K. Nakayama, Y. Hirose, J. Soeda, M. Uno, W. Li, M. Yamagishi, Y. Okada, and J. Takeya, Curr. Appl. Phys. **12**, S87 (2012).

[52] C. Liu, T. Minari, X. Lu, A. Kumatani, K. Takimiya, and K. Tsukagoshi, Adv. Mater. **23**, 523 (2011).

[53] J. Soeda, Y. Hirose, M. Yamagishi, A. Nakao, T. Uemura, K. Nakayama, M. Uno, Y. Nakazawa, K. Takimiya, and J. Takeya, Adv. Mater. **23**, 3309 (2011).

[54] T. Uemura, Y. Hirose, M. Uno, K. Takimiya, and J. Takeya, Appl. Phys. Express **2**, 111501 (2009).

[55] J.-M. Cho and T. Mori, Phys. Rev. Appl. **5**, 064017 (2016).

[56] S.-H. Wen, A. Li, J. Song, W.-Q. Deng, K. L. Han, and W. A. Goddard III, J. Phys. Chem. B **113**, 8813 (2009).

[57] V. Stehr, J. Pfister, R. F. Fink, B. Engels, and C. Deibel, Phys. Rev. B **83**, 155208 (2011).

[58] The effective mass of single-crystal pentacene reported in Ref. [49] is incorrect because the signs of the transfer integrals were not taken into account. In the present paper, we calculated the band mobility using the effective masses of $m_a/m_0 = 7.00$ and $m_b/m_0 = 1.54$, which were obtained in Ref. [32]. We employed the other parameters reported in Ref. [49].

[59] S. A. Arabi, J. Dong, M. Mirza, P. Yu, L. Wang, J. He, and C. Jiang, Cryst. Growth. Des. **16**, 2624 (2016).

[60] Y. Takeyama, S. Ono, and Y. Matsumoto, Appl. Phys. Lett. **101**, 083303 (2012).

[61] J. Y. Lee, S. Roth, and Y. W. Park, Appl. Phys. Lett. **88**, 252106 (2006).

[62] L. B. Roberson, J. Kowalik, L. M. Tolbert, C. Kloc, R. Zeis, X. Chi, R. Fleming, and C. Wilkins, J. Am. Chem. Soc. **127**, 3069 (2005).

[63] T. Uemura, M. Yamagishi, J. Soeda, Y. Takatsuki, Y. Okada, Y. Nakazawa, and J. Takeya, Phys. Rev. B **85**, 035313 (2012).

[64] C. Reese, W.-J. Chung, M.-M. Ling, M. Roberts, and Z. Bao, Appl. Phys. Lett. **89**, 202108 (2006).

[65] C. Goldmann, S. Haas, C. Krellner, K. P. Pernstich, D. J. Gundlach, and B. Batlogg, J. Appl. Phys. **96**, 2080 (2004).

[66] J. Takeya, C. Goldmann, S. Haas, K. P. Pernstich, B. Ketterer, and B. Batlogg, J. Appl. Phys. **94**, 5800 (2003).

[67] V. Y. Butko, X. Chi, D. V. Lang, and A. P. Ramirez, Appl. Phys. Lett. **83**, 4773 (2003).

[68] R. S. Sánchez-Carrera, S. Atahan, J. Schrier, and A. Aspuru-Guzik, J. Phys. Chem. C **114**, 2334 (2010).

[69] W. Xie, K. Willa, Y. Wu, R. Häusermann, K. Takimiya, B. Batlogg, and C. D. Frisbie, Adv. Mater. **25**, 3478 (2013).

[70] S. Haas, Y. Takahashi, K. Takimiya, and T. Hasegawa, Appl. Phys. Lett. **95**, 022111 (2009).

[71] M. Uno, Y. Tominari, M. Yamagishi, I. Doi, E. Miyazaki, K. Takimiya, and J. Takeya, Appl. Phys. Lett. **94**, 223308 (2009).
[72] N. Karl, Synth. Met. **133**, 649 (2003).
[73] C. Mitsui, T. Okamoto, M. Yamagishi, J. Tsurumi, K. Yoshimoto, K. Nakahara, J. Soeda, Y. Hirose, H. Sato, A. Yamano, T. Uemura, and J. Takeya, Adv. Mater. **26**, 4546 (2014).
[74] H. Minemawari, J. Tsurumi, S. Inoue, T. Yamada, R. Kumai, and T. Hasegawa, Appl. Phys. Express **7**, 091601 (2014).
[75] R. A. Marcus, J. Chem. Phys. **24**, 966 (1956).
[76] To our knowledge, the intrinsic mobility calculated from the previous approach using $D^{(x)}(t)$ has never exhibited thermally activated behavior. Flexible surface-hopping approach, a different approach based on the quantum dynamics, can qualitatively reproduce both bandlike transport and hopping transport properties for a one-dimensional model [27].
[77] J. Tsurumi, H. Matsui, T. Kubo, R. Häusermann, C. Mitsui, T. Okamoto, S. Watanabe, and J. Takeya, Nat. Phys. **13**, 994 (2017).